

Universal Behavior of X-ray Flares from Black Hole Systems

F. Y. Wang^{1,2}, Z. G. Dai^{1,2}, S. X. Yi^{1,2} & S. Q. Xi³

¹School of Astronomy and Space Science, Nanjing University, Nanjing 210093, China

²Key Laboratory of Modern Astronomy and Astrophysics (Nanjing University), Ministry of Education, Nanjing 210093, China

³ Department of Physics and GXU-NAOC Center for Astrophysics and Space Sciences, Guangxi University, Nanning 530004, China

ABSTRACT

X-ray flares have been discovered in black hole systems, such as gamma-ray bursts, the tidal disruption event Swift J1644+57, the supermassive black hole Sagittarius A* at the center of our Galaxy, and some active galactic nuclei. Their occurrences are always accompanied by relativistic jets. However, it is still unknown whether there is a physical analogy among such X-ray flares produced in black hole systems spanning nine orders of magnitude in mass. Here we report the observed data of X-ray flares, and show that they have three statistical properties similar to solar flares, including power-law distributions of energies, durations, and waiting times, which both can be explained by a fractal-diffusive self-organized criticality model. These statistical similarities, together with the fact that solar flares are triggered by a magnetic reconnection process, suggest that all of the X-ray flares are consistent with magnetic reconnection events, implying that their concomitant relativistic jets may be magnetically dominated.

Subject headings: accretion, accretion discs–black hole physics–gamma-ray burst: general–radiation mechanism: non-thermal

1. Introduction

X-ray flares are common astrophysical explosive phenomena throughout the universe. They have been observed in stars, stellar-mass black holes, and supermassive black holes (SMBHs) located at the center of galaxies, particularly in the Sun (Shibata & Magara 2011), gamma-ray bursts (GRBs) (Gehrels et al. 2009), the tidal disruption event Swift J1644+57

E-mail: fayinwang@nju.edu.cn; dzg@nju.edu.cn

(Burrows et al. 2011; Bloom et al. 2011), the SMBH Sagittarius A* (named Sgr A*) at the center of our Galaxy (Baganoff et al. 2001), and some active galactic nuclei (AGN) (Rees 1984). These black hole systems, spanning nine orders of magnitude in mass, always generate relativistic jets (De Young 1991; Mirabel & Rodriguez 1999; Meier et al. 2001; Zhang 2007), which are likely to produce X-ray flares with short rise and decay times. Until now, the composition of such relativistic jets has been poorly known (Harris & Krawczynski 2006). Meanwhile the physical origin of resultant X-ray flares has also remained mysterious, although some models have been proposed for X-ray flares in GRBs (Dai et al. 2006; Mészáros 2006), Swift J1644+57 (Wang & Cheng 2012), Sgr A* (Markoff et al. 2001; Yuan et al. 2003; Yuan et al. 2004; Dodds-Eden et al. 2010), and M87 (Harris et al. 2003). It is well known that solar flares originate from magnetic reconnection (Shibata & Magara 2011; Zweibel & Yamada 2009). Here we investigate the energy frequency distribution, duration-time distribution and waiting time distribution of X-ray flares from black hole systems, compare these distributions with those of solar flares, and infer the physical origin of X-ray flares and the composition of relativistic jets.

In astrophysics, there is consensus about a common set of morphological properties, which may be shared by most of X-ray flares spanning many orders of magnitude in power. Interestingly, there is evidence that GRB X-ray flares and solar flares have similar statistical properties, suggesting a similar physical origin, i.e. magnetic reconnection (Wang & Dai 2013). However, a clear connection among X-ray flares from relativistic jets in black hole systems with vastly different masses has not yet been built, though a recent study shows that relativistic jets in GRBs and AGNs may have a similar efficiency of energy dissipation (Nemmen et al. 2012). Wang et al. (2014) found that the correlation between radio luminosity and peak energy of GRBs is similar as that of blazars, which indicated that the radiation process of GRBs is synchrotron radiation both in the prompt and afterglow phases.

Solar flares are believed to be self-organized criticality (SOC) events driven by magnetic reconnection (Lu & Hamilton 1991; Charbonneau et al. 2001; Morales & Charbonneau 2008; Aschwanden 2012a). The concept of SOC was first proposed by Bak et al. (1987, 1988), which has been initially applied to sandpile avalanches, and has been generalized to nonlinear dissipative systems that are driven in a critical state. Wang & Dai (2013) found that X-ray flares from GRBs show SOC behaviors. Whether the SOC characteristics exist in X-ray flares in black hole systems except for GRBs remains unclear, though some hints have been found (Mineshige et al. 1994; Takeuchi et al. 1995; Negoro et al. 1995; Ciprini et al. 2003; Zhang 2007).

In this paper, we study the energy frequency distribution, duration-time distribution and waiting time distribution of X-ray flares from black hole systems, such as Swift J1644+57,

Sgr A* and M87. The structure of this paper is arranged as follows. In section 2, we derive the X-ray flare data. We present the fitting results and explanations in section 3. The conclusions and discussion are given in section 4.

2. The X-ray flare data

We focus on X-ray flares from SMBHs, such as the central black hole of Swift J1644+57, Sgr A* at our Galactic center, and the AGN M87.

2.1. X-ray flares of Swift J1644+57

Swift J1644+57 is the first event with a relativistic jet generated by the tidal disruption of a star by a SMBH (Burrows et al. 2011; Bloom et al. 2011). This event is at redshift $z = 0.35$. The central black hole mass of Swift J1644+57 is about $7.4 \times 10^6 M_\odot$ (Burrows et al. 2011), where M_\odot is the solar mass. There are many flares presented in the X-ray light curve of Swift J1644+57 (Burrows et al. 2011). The X-ray light curve of Swift J1644+57 is obtained from http://www.swift.ac.uk/xrt_curves (Evans et al. 2007), which was observed by the Swift satellite (Gehrels et al. 2004). The X-ray flux in the 0.3-10 keV band is shown in Figure 1. The X-ray telescope (XRT) on board Swift has a number of different operating modes, depending on the brightness of an observed source. The time resolution is from millisecond to seconds (Gehrels et al. 2004). The data are binned dynamically, i.e., the binning criteria vary with count rate (Evans et al. 2007). The solid line represents the underlying continuum emission, which is dramatically consistent with the Chandra X-ray observations in about 500 days when the relativistic jet shuts off (Zauderer et al. 2013). When we fit the parameters of flares, the underlying continuum emission is subtracted. The total X-ray emission shows a constant flux at $t < 15$ days (Burrows et al. 2011) and $F_X \propto t^{-5/3}$ at $t > 15$ days (Berger et al. 2012). The constant flux may be due to the extraction of the rotational energy of a spinning supermassive black hole through the Blandford-Znajek mechanism (Blandford & Znajek 1977; Lei & Zhang 2011). The steady decline $F_X \propto t^{-5/3}$ traces the mass accretion rate of post-disruption debris (Rees 1988). We fit the flares with a smooth broken power-law function (Li et al. 2012)

$$F(t) = F_0 \left[\left(\frac{t}{t_b} \right)^{\alpha_1 \omega} + \left(\frac{t}{t_b} \right)^{\alpha_2 \omega} \right]^{-\frac{1}{\omega}}, \quad (1)$$

where α_1 and α_2 are the temporal slopes, t_b is the break time, and ω measures the sharpness of a peak of the light curve component. This method is very similar to the fitting method of

GRB X-ray flares (Chincarini et al. 2007; Chincarini et al. 2010; Falcone et al. 2007). The example of best-fit flares is shown in Figure 2. The flare parameters including the start time, end time, fluence, fluence error and isotropic energy are shown in Table 1. The total number of X-ray flares of Swift J1644+57 is 68. These parameters are derived as follows. The isotropic energy of one flare in the 0.3-10 keV band can be calculated by $E_{\text{iso}} = 4\pi d_L^2(z) S_F / (1+z)$, where S_F is the fluence, $z = 0.35$ is the redshift, and $d_L(z)$ is the luminosity distance calculated for a flat Λ CDM universe with $\Omega_M = 0.3$, $\Omega_\Lambda = 0.7$ and $H_0 = 70 \text{ km s}^{-1} \text{ Mpc}^{-1}$. The error of flare energy is calculated by $\sigma_E = 4\pi d_L^2(z) \sigma_{S_F} / (1+z)$, where σ_{S_F} is the error of fluence. The waiting time in the source’s rest frame can be obtained by $\Delta t = (t_{i+1} - t_i) / (1+z)$, where t_{i+1} is the observed start time of the $i+1$ th flare, t_i is the observed start time of the i th flare, and $1+z$ is the factor to transfer the time into the source-frame one. The duration time is calculated as $T = (t_{\text{end}} - t_{\text{start}}) / (1+z)$.

2.2. X-ray flares of Sgr A*

The SMBH Sgr A* at our Galactic center has a mass of $4.1 \times 10^6 M_\odot$ at its distance of 8 kiloparsecs to the Earth (Ghez et al. 2008). Sgr A* shows flares in the X-ray and near infrared bands (Dodds-Eden et al. 2009). The X-ray emission of Sgr A* typically has a luminosity of a few times $10^{33} \text{ erg s}^{-1}$ (Baganoff et al. 2003), but it shows rapid X-ray flaring sometimes. Here we use the observational data from the Chandra X-ray Observatory’s 2012 Sgr A* X-ray Visionary Project (Wang et al. 2013). In 3 mega-seconds of Chandra observations, 39 X-ray flares from Sgr A* with duration from a few hundred seconds to 8000 seconds and with 2-10 keV luminosity from $10^{34} \text{ erg s}^{-1}$ to $2 \times 10^{35} \text{ erg s}^{-1}$ were detected (Neilsen et al. 2013). The flare parameters of Sgr A* are compiled in Table 2, which are taken from (author?) (Neilsen et al. 2013). The underlying emission is subtracted when the parameters of flares are derived (Neilsen et al. 2013). The waiting time is calculated from $\Delta t = (t_{i+1} - t_i)$, where t_{i+1} is the observed start time of the $i+1$ th flare, t_i is the observed start time of the i th flare. Neilsen et al. (2013) found that the X-ray flare luminosity distribution dN/dL is consistent with a power law with index about -1.9 , and the duration time distribution is a power law with index -0.9 ± 0.2 .

2.3. X-ray flares of M87

The first jet was discovered in 1918 within the elliptical galaxy M87 in the Virgo cluster. M87 shows X-ray flaring from nucleus, HST-1, knot A, and knot D. The very high-energy ($E > 100 \text{ GeV}$) flares have been detected. In this study, we use the X-ray light curve

for the nucleus of M87 observed by Chandra between 2000 and 2010 (Harris et al. 2009; Abramowski et al. 2012). X-ray data of M87 have been taken with the Advanced CCD Imaging Spectrometer (ACIS) on board the Chandra satellite (Harris et al. 2003; Harris et al. 2009; Abramowski et al. 2012), which is shown in Figure 3. The underlying emission is about 0.1 keV/s (Harris et al. 2009), which is subtracted when we derive the parameters. We identify 18 flares from the X-ray light curve. The parameters of flares are listed in Table 3, including the start time, end time and energy. We take the error as 15% of total energy.

3. Results

We present the cumulative energy distribution of X-ray flares in Figure 4. The number of flares $N(E)dE$ with energy between E and $E + dE$ can be expressed by

$$N(E)dE \propto E^{-\alpha_E} dE \quad E < E_{\max}, \quad (2)$$

where α_E is the power-law index, and E_{\max} is the cutoff energy. So the cumulative energy distribution is $N(> E) = a + b[E^{1-\alpha_E} - E_{\max}^{1-\alpha_E}]$, where a and b are two parameters. We use the Markov chain Monte Carlo technique to obtain the best-fitting parameters. The distribution shows a flat part at the low energy regime, which may be due to an incomplete sampling and some selection bias for large energy flares. Interestingly, Cliver et al. (2012) also interpreted the flatter slope of solar energetic particle events using selection effects. So in order to avoid the selection effect, only the cumulative distribution above the break is fitted. The flattening effect due to the incomplete sampling is well understood. In Figure 4, we fit the cumulative distributions in the energy range between the dashed lines. Because the number of solar flares is very large, we fit the differential distribution with $\alpha_E = 1.65 \pm 0.02$ for 11595 solar flares observed by RHESSI (Aschwanden 2011). The other red curves in Figure 4 represent the cumulative energy distributions of X-ray flares with indices $\alpha_E = 2.4 \pm 0.6$, 1.8 ± 0.6 , and 1.6 ± 0.7 for Swift J1644+57, Sgr A*, and M87, respectively. The reduced χ^2 of fittings are $\chi_r^2 = 1.02$, 0.83, 0.85, and 0.75 for solar flares, Swift J1644+57, Sgr A*, and M87, respectively. Neilsen et al. (2013) also fitted the energy of Sgr A* flares using a cutoff power-law function. The best fitting slope is $0.9^{+0.8}_{-0.5}$, which is in contrast with our result. The main reason is that the incomplete sampling at low energy range. Figure 5 shows the duration-time (T) frequency distributions X-ray flares from black hole systems. The differential distribution can be expressed as

$$N(T)dT \propto T^{-\alpha_T} dT. \quad (3)$$

Because the number of flares from black hole systems is small. We also use the cumulative distribution, which is the integration of equation (3). In order to avoid the incomplete

sampling problem, the distribution above the break point is fitted, which is between dashed lines in Figure 5. The values of α_T are 2.00 ± 0.05 , 1.5 ± 0.6 , 1.9 ± 0.5 , and 2.0 ± 0.7 for solar flares, Swift J1644+57, Sgr A*, and M87, respectively. The reduced χ^2 of fittings are $\chi_r^2 = 0.98, 0.83, 0.86$, and 0.74 for solar flares, Swift J1644+57, Sgr A*, and M87, respectively. The fitting results are listed in Table 4. Because the flares are from the same object observed by the same instrument, the observational bias may be minimal.

Obviously, the typical values of α_E are about 1.6 and 2.4, and those of α_T are about 2.0 and 1.5. Some distributions of flares can be well understood within one physical framework, i.e., self-organized criticality (SOC). The concept of SOC was proposed as an explanation for the behavior of the sandpile model (Bak et al. 1987). In SOC, subsystems self-organize owing to some driving force to a critical state at which the “output” is a series of “avalanches” that follow a power-law (fractal) frequency-size distribution. For solar flares, the statistical power-law distributions of sizes and durations can be explained by the universal fractal-diffusive SOC model (Aschwanden 2011; Aschwanden 2012a), while the underlying physical process of the driver could be attributed to a magnetic reconnection process. We further discuss this model to explain the energy and duration-time frequency distributions of X-ray flares in other systems. For an ensemble of many SOC avalanches, the relationship between size scale L and duration time T is $L \propto T^{1/2}$ (Aschwanden 2012a), which has been originally applied to the Brownian motion. This relationship has been confirmed by the observations of solar flares (Aschwanden 2012b). Meanwhile, under the assumption that the number or occurrence frequency of avalanches is equally likely throughout the system, the distribution of size scale L is expressed as $N(L)dL \propto L^{-S}dL$, where $S = 1, 2$ and 3 is the Euclidean dimension. Thus, the duration frequency distribution of flares is given by (Aschwanden 2012a)

$$N(T)dT \propto T^{-(S+1)/2}dT. \quad (4)$$

For $S = 3$, the index $\alpha_T = (S + 1)/2$ equals 2.0, which can well reproduce the duration frequency distributions of X-ray flares of Sun, Sgr A*, and M87 at the 1σ confidence level. In addition, the energy frequency distribution can be expressed as (Aschwanden 2012a)

$$N(E)dE \propto E^{-3(S+1)/(S+5)}dE. \quad (5)$$

The index $\alpha_E \equiv 3(S+1)/(S+5) = 1.5$ for $S = 3$, which is consistent with the observed indices of X-ray flares of Sun, Sgr A*, and M87. The power-law distributions of total energies and durations are two criteria of a SOC system (Aschwanden 2011). From our above statistical analysis, the X-ray flares from Sun, Sgr A*, and M87 are due to SOC events. The X-ray flares of Sun, Sgr A*, and M87 correspond to the three-dimensional ($S = 3$) case. Interestingly, Li & Yuan (2014) also found that the distributions of Sgr A* flares, including flux, peak rate and waiting time, can be explained by three-dimensional fractal-diffusive SOC model. The best

fitting power-law slopes are $\alpha_E = 2.4 \pm 0.6$ and $\alpha_T = 1.5 \pm 0.6$ for Swift J1644+57. According to the fractal-diffusive SOC model proposed by Aschwanden (2012a), these power-law slopes can be marginally explained by the three-dimensional SOC model. But the difference is up to 0.6. Interestingly, the size distributions of stellar flare energies with power-law slopes in a range of $\alpha_E = 2.17 \pm 0.25$ (Aschwanden 2014). For stellar flares from Kepler mission, the size distribution for the total sample of 1538 stellar flares shows a power law slope of $\alpha_E = 2.04 \pm 0.13$ (Walkowicz et al. 2011; Maehara et al. 2012; Shibayama et al. 2013; Aschwanden 2014). These values are dramatically consistent with our result, but are steeper than derived for solar flare energies ($\alpha_E \approx 1.5 - 1.6$).

The waiting time Δt is the time interval between two successive events in a data set. Figure 6 shows the waiting time distributions of X-ray flares from the Sun, Swift J1644+57, Sgr A* and M87, which suggests that these X-ray flares have similar waiting-time distributions. The power-law indices of waiting-time distributions α_W are 2.04 ± 0.03 , 1.8 ± 0.6 , 1.8 ± 0.9 , and 2.9 ± 1.0 for solar flares, Swift J1644+57, Sgr A*, and M87, respectively. The corresponding reduced χ^2 are $\chi_r^2 = 0.96$, 0.83, 0.79, and 0.70 for solar flares, Swift J1644+57, Sgr A*, and M87, respectively. The power-law waiting time distributions of X-ray flares can be explained by non-stationary Poisson processes (Wheatland et al. 1998; Aschwanden & McTiernan 2010). The power-law index α_W of waiting time distribution is dependent on the flare rate. For the flare rate distribution

$$f(\lambda) = \lambda^{-1} \exp(-\lambda/\lambda_0) \quad (6)$$

with flare rate $\lambda = 1/\Delta t$ and mean rate λ_0 , the waiting time distribution can be derived as (Aschwanden & McTiernan 2010)

$$P(\Delta t) = \frac{\lambda_0}{(1 + \lambda_0 \Delta t)^2}, \quad (7)$$

where λ_0 is the mean rate of flares. For waiting times ($\Delta t \gg 1/\lambda_0$), equation 7 approaches a power-law limit $P(\Delta t) \approx (1/\lambda_0)(\Delta t)^{-2}$, which is consistent with solar flares, GRBs and Sgr A*. Next, we consider the flare rate distribution with a mean rate λ_0

$$f(\lambda) = \frac{1}{\lambda_0} \exp(-\lambda/\lambda_0), \quad (8)$$

defined in the range of $0 < \lambda < \infty$. In this case, the waiting time distribution can be written as (Aschwanden & McTiernan 2010)

$$P(\Delta t) = \int_0^\infty (-\lambda/\lambda_0)^2 \exp\left[-\frac{\lambda}{\lambda_0}(1 + \lambda_0 \Delta t)\right] d\lambda. \quad (9)$$

This equation corresponds to the integral $\int_0^\infty x^2 e^{ax} dx = -2/a^3$, with $a = -(1 + \lambda_0 \Delta t)/\lambda_0$. So the waiting time distribution is

$$P(\Delta t) = \frac{2\lambda_0}{(1 + \lambda_0 \Delta t)^3}. \quad (10)$$

Obviously, the power-law index approaches -3 for $\Delta t \gg 1/\lambda_0$, which is remarkably consistent with the X-ray flares of M87.

4. Conclusions and discussion

In this paper, we study the statistical properties of X-ray flares from different objects. The best fitting results for the distributions of energy, duration and waiting time are shown in Table 4. The statistical similarities among X-ray flares from the Sun, GRBs, Swift J1644+57, Sgr A*, and M87, suggest that all of the X-ray flares have a similar physical origin, i.e., magnetic reconnection. Our results show that X-ray flares from Sun, Sgr A*, and M87 can be explained by a three-dimensional SOC model, implying that relativistic jets may be magnetically dominated. The power-law slopes of Swift J1644+57 distributions can be marginally explained in the three-dimensional SOC case. But the difference is up to 0.6. X-ray flares in black hole systems may occur in the following way. The central engine first ejects a relativistic magnetically-dominated jet (Meier et al. 2001), and subsequently, blobs with different velocities in such a jet collide with each other (Yuan & Zhang 2012), triggering magnetic reconnection events. Finally, relativistic electrons accelerated in the jet, owing to these events, emit X-ray flares. In addition, our results also show that SOC events are common phenomena in our universe, from local to distant objects and from the Sun with $1M_\odot$ to M87 with a few $10^9 M_\odot$. This will possibly motivate further studies of astrophysical SOC events.

Acknowledgements

We thank the two referees for detailed and very constructive suggestions that have allowed us to improve our manuscript. We thank M. J. Aschwanden, L. A. Balona, P. F. Chen, M. D. Ding, Y. F. Huang, X. Y. Wang, F. Yuan, and S. N. Zhang for their discussions. This work is supported by the National Basic Research Program of China (973 Program, grant No. 2014CB845800), the National Natural Science Foundation of China (grants 11422325, 11373022, 11103007, and 11033002), the Excellent Youth Foundation of Jiangsu Province (BK20140016), and the Program for New Century Excellent Talents in

University (grant No. NCET-13-0279). This work made use of data supplied by the UK Swift Science Data Center at the University of Leicester.

REFERENCES

- Abramowski, A. et al., 2012, *ApJ*, 746, 151
- Aschwanden, M. J., 2011, *Self-Organized Criticality in Astrophysics: The Statistics of Non-linear Processes in the Universe*, Springer-Verlag: Berlin
- Aschwanden, M. J., 2012a, *A&A*, 539, A2
- Aschwanden, M. J., 2012b, *ApJ*, 757, 94
- Aschwanden, M. J., 2014, *ApJ*, 782, 54
- Aschwanden, M. J. & McTiernan, J. M., 2010, *ApJ*, 717, 683
- Baganoff, F. K., Bautz, M. W., Brandt, W. N., et al., 2001, *Nature*, 413, 45
- Baganoff, F. K., Maeda, Y., Morris, M., et al., 2003, *ApJ*, 591, 891
- Bak, P. Tang, C. & Wiesenfeld, K., 1987, *Phys. Rev. Lett.*, 59, 381
- Bak, P. Tang, C. & Wiesenfeld, K., 1988, *Phys. Rev. A*, 38, 364
- Berger, E., Zauderer, A., Pooley, G. G., Soderberg, A. M., Sari, R., Brunthaler, A. & Bietenholz, M. F., 2012, *ApJ*, 748, 36
- Blandford, R. D. & Znajek, R. L., 1977, *MNRAS*, 179, 433
- Bloom, J. S., Giannios, D., Metzger, B. D., et al., 2011, *Science*, 333, 203
- Burrows, D. N., Kennea, J. A., Ghisellini, G., et al., 2011, *Nature*, 476, 421
- Charbonneau, P. S. W., McIntosh, W. W., Liu, H.-L., & Bogdan, T. J. 2001, *Sol. Phys.*, 203, 321
- Cheng, B. L., Epstein, R. I., Guyer, R. A. & Young, A. C., 1996, *Nature*, 382, 518
- Chincarini, G., Moretti, A., Romano, P., et al., 2007, *ApJ*, 671, 1903
- Chincarini, G., Mao, J., Margutti, R., et al., 2010, *MNRAS*, 406, 2113

- Ciprini, S., Fiorucci, M., Tosti, G., & Marchili, N., 2003, High energy blazar astronomy, ASP Conf. Proc. 229, ASP: San Francisco, p. 265
- Cliver, E. W., Ling, A. G., Belov, A. & Yashiro, S., 2012, ApJ, 756, L29
- Dai, Z. G., Wang, X. Y., Wu, X. F. & Zhang, B., 2006, Science, 311, 1127
- De Young, D. S. 1991, Science, 252, 389
- Dodds-Eden, K., Porquet, D., Trap, G., et al., 2009, ApJ, 698, 676
- Dodds-Eden, K., Sharma, P., Quataert, E., Genzel, R., Gillessen, S., Eisenhauer, F. & Porquet, D. et al., 2010, ApJ, 725, 450
- Evans, P. A., Beardmore, A. P., Page, K. L., et al., 2007, A&A, 469, 379
- Falcone, A. D., Morris, D., Racusin, J., et al., 2007, ApJ, 671, 1921
- Gehrels, N., Chincarini, G., Giommi, P., et al., 2004, ApJ, 611, 1005
- Gehrels, N., Ramirez-Ruiz, E., & Fox, D. B. 2009, ARA&A, 47, 567
- Ghez, A. M., Salim, S., Weinberg, N. N., et al., 2008, ApJ, 689, 1044
- Harris, D. E., Biretta, J. A., Junor, W., Perlman, E. S., Sparks, W. B. & Wilson, A. S., 2003, ApJ, 586, L41
- Harris, D. E., Cheung, C. C., Stawarz, L., Biretta, J. A. & Perlman, E. S., 2009, ApJ, 699, 305
- Harris, D. E. & Krawczynski, H., 2006, ARA&A, 44, 463
- Lei, W. H. & Zhang, B., 2011, ApJ, 740, L27
- Li, L., Liang, E. W., Tang, Q. W., et al., 2012, ApJ, 758, 27
- Li, Y. P. & Yuan, F., 2014, submitted
- Lu, E. T. & Hamilton, R. J., 1991, ApJ, 380, L89
- Maehara, H., Shibayama, T., Notsu, S., et al. 2012, Nature, 485, 478
- Markoff, S., Falcke, H., Yuan, F. & Biermann, P. L., 2001, A&A, 379, L13
- Meier, D. L., Koide, S. & Uchida, Y. 2001, Science, 291, 84

- Mészáros, P., 2006, *Rep. Prog. Phys.*, 69, 2259
- Mineshige, S., Ouchi, N. B., & Nishimori, H., 1994, *PASJ*, 46, 97
- Mirabel, I. F. & Rodriguez, L. F., 1999, *ARA&A*, 37, 409
- Morales, L., & Charbonneau, P. 2008, *ApJ*, 682, 654
- Negoro, H., Kitamoto, S., Takeuchi, M., & Mineshige, S., 1995, *ApJ*, 452, L49
- Neilsen, J., Nowak, M. A., Gammie, C., et al., 2013, *ApJ*, 774, 42
- Nemmen, R. S., Georganopoulos, M., Guiriec, S., Meyer, E. T., Gehrels, N. & Sambruna, R. M., 2012, *Science*, 338, 1445
- Rees, M. J. 1984, *ARA&A*, 22, 471
- Rees, M. J., 1988, *Nature*, 333, 523
- Shibata, K., & Magara, T., 2011, *Living Rev. Solar Phys.*, 8, 6
- Shibayama, T., Maehara, H., Notsu, S., et al. 2013, *ApJS*, 209, 5
- Takeuchi, M., Mineshige, S., & Negoro, H., 1995, *PASJ*, 47, 617
- Walkowicz, L. M., Basri, G., Batalha, N., et al. 2011, *AJ*, 141, 50
- Wang, Q. D., Nowak, M. A., Markoff, S. B., et al., 2013, *Science*, 341, 981
- Wang, F. Y. & Cheng, K. S., 2012, *MNRAS*, 421, 908
- Wang, F. Y. & Dai, Z. G., 2013, *Nature Phys.*, 9, 465
- Wang, F. Y., Yi, S. X. & Dai, Z. G., 2014, *ApJL*, 786, L8
- Wheatland, M. S., Sturrock, P. A. & McTiernan, J. M., 1998, *ApJ*, 509, 448
- Yuan, F., Quataert, E. & Narayan, R., 2003, *ApJ*, 598, 301
- Yuan, F., Quataert, E. & Narayan, R., 2004, *ApJ*, 606, 894
- Yuan, F. & Zhang, B., 2012, *ApJ*, 757, 56
- Zhang, S. N., 2007, *Highlights of Astronomy*, 14, 41
- Zauderer, B. A., Berger, E., Margutti, R., et al., 2013, *ApJ*, 767, 152

Zweibel, E. G. & Yamada, M., 2009, *ARA&A*, 47, 291

Table 1. The measured parameters of X-ray flares of Swift J1644+57.

$t_{\text{start}}^{\text{a}}$ (s)	$t_{\text{end}}^{\text{b}}$ (s)	S_F^{c} (10^{-8} erg cm $^{-2}$)	$\sigma_{S_F}^{\text{d}}$ (10^{-8} erg cm $^{-2}$)	$E_{\text{iso}}^{\text{e}}$ (10^{50} ergs)
2019.2	2814.3	36.4	8.2	1.10
17750.2	27267.8	17.7	5.3	0.53
33099.6	50059.5	129.5	25.2	3.90
45489.5	49643.7	73.7	15.0	2.22
39025.2	1.71E5	128.7	32.3	3.88
75411.5	90710.2	23.6	6.1	0.71
1.10E5	1.12E5	13.6	3.2	0.41
1.108E5	1.116E5	3.37	1.4	0.102
1.109E5	1.469E5	88.2	17.6	2.66
1.121E5	1.129E5	6.48	1.5	0.195
1.331E5	1.602E5	132.6	27.3	3.99
1.393E5	1.422E5	12.39	2.4	0.373
1.397E5	1.401E5	6.89	1.4	0.208
1.391E5	1.445E5	142.5	35.0	4.30
1.451E5	1.472E5	9.91	2.4	0.299
1.455E5	1.476E5	16.18	4.1	0.488
1.729E5	2.264E5	57.81	12.3	1.742
1.738E5	1.894E5	15.89	3.5	0.479
1.852E5	1.912E5	6.00	1.4	0.181
1.869E5	1.947E5	147.5	37.9	4.45
2.028E5	2.216E5	24.50	5.3	0.738
2.085E5	2.195E5	95.87	21.3	2.89
2.154E5	3.516E5	173.1	38.2	5.22
2.666E5	3.017E5	83.14	13.4	2.51
2.955E5	4.198E6	3496.2	450.1	105.4
3.172E5	3.667E5	162.4	31.7	4.89
3.901E5	5.377E5	326.0	50.6	9.83
5.236E5	9.966E5	495.6	89.8	14.94
6.020E5	6.109E5	15.24	3.2	0.459
6.184E5	6.291E5	24.61	4.3	0.742
7.642E5	9.235E5	545.5	97.3	16.44
9.557E5	1.562E6	1444.3	201.5	43.53
1.204E6	1.333E6	620.8	80.4	18.71
1.309E6	1.394E6	116.7	20.0	3.52

1.363E6	1.447E6	85.20	25.8	2.57
1.459E6	1.461E6	3.79	0.9	0.114
1.463E6	1.543E6	115.9	20.3	3.49
1.436E6	1.597E6	242.1	35.2	7.30
1.540E6	1.965E6	996.8	130.6	30.04
1.856E6	2.059E6	247.8	37.8	7.47
2.067E6	2.307E6	294.6	40.0	8.88
2.280E6	3.581E6	428.0	89.7	12.90
2.342E6	2.524E6	60.30	15.3	1.82
2.442E6	2.562E6	255.9	63.4	7.71
2.597E6	3.481E6	378.7	78.2	11.41
2.780E6	2.875E6	108.4	30.8	3.27
2.942E6	3.727E6	377.3	64.2	11.37
3.188E6	3.246E6	100.9	20.4	3.04
3.188E6	3.691E6	1289.9	300.2	38.87
3.599E6	3.986E6	228.8	46.2	6.89
4.007E6	4.360E6	109.2	18.9	3.29
4.335E6	4.536E6	159.7	31.8	4.81
4.404E6	4.987E6	353.2	83.2	10.65
5.336E6	6.246E6	291.4	50.7	8.78
6.065E6	6.195E6	19.35	5.8	0.583
6.064E6	7.228E6	437.7	67.4	13.19
7.142E6	7.314E6	20.60	5.2	0.62
7.029E6	7.979E6	257.0	63.8	7.75
7.942E6	8.265E6	64.7	13.5	1.95
8.359E6	8.562E6	23.32	6.1	0.70
8.293E6	1.250E7	344.3	69.5	10.38
9.326E6	9.869E6	39.2	7.3	1.18
9.329E6	1.437E7	366.7	73.8	11.05
9.773E6	1.295E7	870.3	143.8	26.23
1.297E7	2.511E7	199.1	45.2	6.00
1.426E7	1.712E7	516.2	34.9	15.56
1.635E7	3.996E7	607.5	130.2	18.31
2.528E7	9.447E7	343.2	65.2	10.34

Note: (a) The start time of a flare. (b) The end time of a flare. (c) The fluence of flare.
(d) The error of fluence. (e) The flare energy.

Table 2: The parameters of X-ray flares of Sgr A*. Note: (a) The start time of a flare in units of Modified Julian Date (MJD). (b) The end time of flare in units of MJD. (c) The fluence of flares. (d) The duration of flares.

$t_{\text{start}}^{\text{a}}$ (MJD)	$t_{\text{end}}^{\text{b}}$ (MJD)	S_F^{c} (cts)	T^{d} (s)	L_{2-10}^{unabs} (10^{34} erg s $^{-1}$)
55966.433	55966.464	33^{+12}_{-11}	2600	1.7
55966.603	55966.666	706^{+46}_{-44}	5450	19.2
56006.486	56006.493	32^{+11}_{-9}	600	7.4
56006.524	56006.540	40^{+12}_{-10}	1350	4.1
56006.580	56006.599	49^{+13}_{-12}	1600	4.2
56006.678	56006.690	49^{+13}_{-14}	950	7.1
56048.510	56048.548	59^{+16}_{-14}	3250	2.5
56048.679	56048.693	15^{+8}_{-7}	1200	1.7
56054.107	56054.154	49^{+15}_{-13}	4050	1.6
56058.687	56058.705	24^{+10}_{-11}	1600	2.0
56059.006	56059.044	33^{+15}_{-11}	3250	1.4
56059.314	56059.329	21^{+10}_{-8}	1250	2.3
56060.127	56060.168	124^{+21}_{-19}	3500	4.9
56067.863	56067.888	102^{+18}_{-17}	2150	6.6
56122.650	56122.656	8^{+6}_{-4}	500	2.3
56126.979	56127.038	58^{+16}_{-15}	5100	1.6
56127.172	56127.202	26^{+11}_{-9}	2550	1.4
56128.549	56128.553	29^{+10}_{-9}	400	10.2
56130.182	56130.225	101^{+19}_{-17}	3700	3.8
56130.906	56130.921	46 ± 13	1300	4.8
56131.494	56131.585	119^{+23}_{-21}	7800	2.1
56132.385	56132.399	38 ± 12	1150	4.5
56133.512	56133.521	14^{+8}_{-7}	750	2.6
56133.997	56134.042	251^{+28}_{-26}	3950	8.9
56139.368	56139.417	166^{+24}_{-22}	4250	5.4
56141.009	56141.035	135^{+21}_{-23}	2250	8.4
56143.314	56143.332	58 ± 15	1550	5.1
56144.321	56144.363	33^{+14}_{-12}	3600	1.2
56147.131	56147.151	27^{+11}_{-10}	1750	2.1
56207.174	56207.194	30^{+11}_{-10}	1700	2.4
56208.187	56208.222	54^{+15}_{-13}	2950	2.5
56216.239	56216.248	58^{+14}_{-12}	750	10.7
56217.094	56217.098	15^{+8}_{-6}	400	5.4
56217.816	56217.884	372^{+34}_{-32}	5900	8.9
56223.384	56223.464	193^{+26}_{-24}	6900	3.8
56225.230	56225.263	63^{+16}_{-14}	2800	3.1
56230.288	56230.362	74^{+19}_{-18}	6350	1.6
56230.734	56230.734	12^{+8}_{-7}	900	2.0

Table 3: The parameters of X-ray flares of M87. Note: (a) The start time of a flare. (b) The end time of a flare. (c) The flare energy.

$t_{\text{start}}^{\text{a}}$ (year)	$t_{\text{end}}^{\text{b}}$ (year)	E^{c} (10^{47} ergs)
1999.3169	2003.4192	9.06
2001.3497	2004.4083	6.05
2002.3079	2007.8254	2.02
2002.7067	2003.8173	2.05
2003.3964	2004.1254	1.92
2003.6656	2004.8537	3.53
2004.3156	2005.2375	1.00
2004.4449	2006.3123	3.72
2005.1603	2005.3801	3.58
2005.2945	2005.6828	1.99
2005.4406	2006.4997	0.11
2006.2941	2007.4452	0.40
2006.9754	2007.9632	6.83
2006.9998	2007.6756	1.41
2007.4370	2008.4702	2.17
2008.0289	2010.7990	0.11
2008.1739	2009.0230	10.1
2008.1969	2010.3154	2.35

Table 4: The properties of X-ray flares.

Source	flare energy (ergs)	number of flares	α_E	α_T	α_W	dimension
Sun	10^{26} - 10^{32}	11595	1.65 ± 0.02	2.00 ± 0.05	2.04 ± 0.03	$S = 3$
GRBs	10^{48} - 10^{52}	83	1.1 ± 0.2	1.1 ± 0.2	1.8 ± 0.2	$S = 1$
Swift J1644+57	10^{48} - 10^{52}	68	2.4 ± 0.6	1.5 ± 0.6	1.8 ± 0.6	$S = 3?$
Sgr A*	10^{37} - 10^{40}	39	1.8 ± 0.6	1.9 ± 0.5	1.8 ± 0.9	$S = 3$
M87	10^{46} - 10^{48}	18	1.6 ± 0.7	2.0 ± 0.7	2.9 ± 1.0	$S = 3$

Note: α_E , α_T , and α_W are the power-law indices of the frequency distributions of flare energies, durations, and waiting times, respectively.

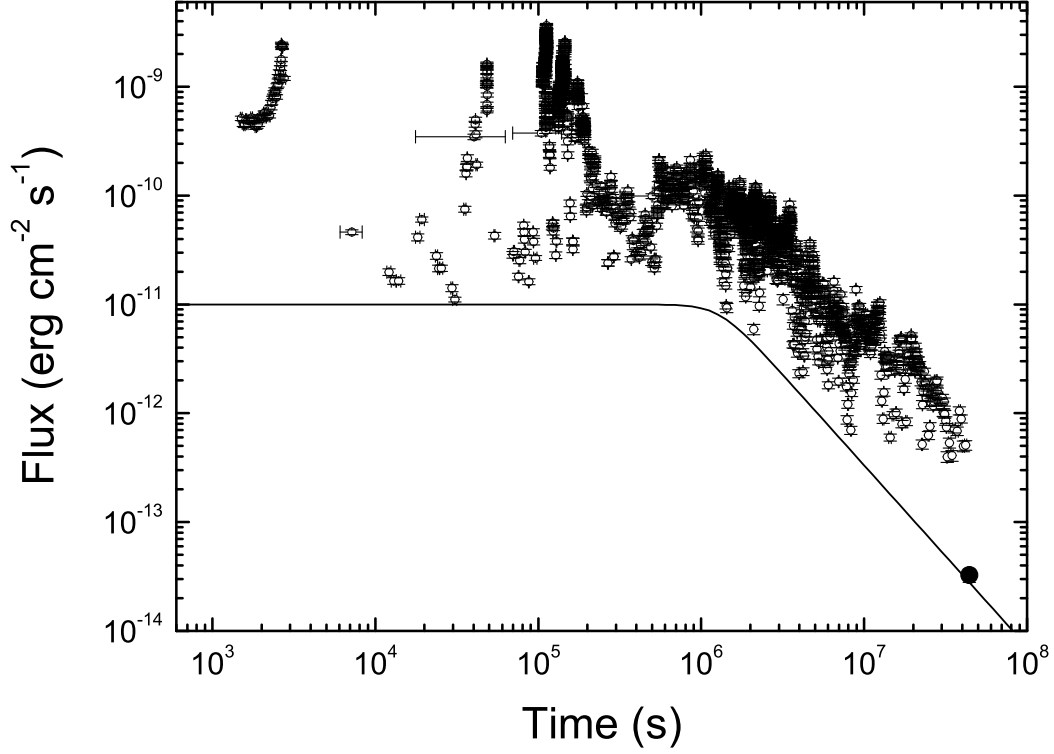


Fig. 1.— X-ray light curve of Swift J1644+57 from Swift/XRT (open circles) and a late-time Chandra observation (filled circle). The black line is the underlying continuum emission with a constant flux at $t < 15$ days and $F_X \propto t^{-5/3}$ at $t > 15$ days. After the relativistic jet shuts off, the underlying continuum emission is consistent with the Chandra observation. The underlying continuum emission has been subtracted when we fit the parameters of flares.

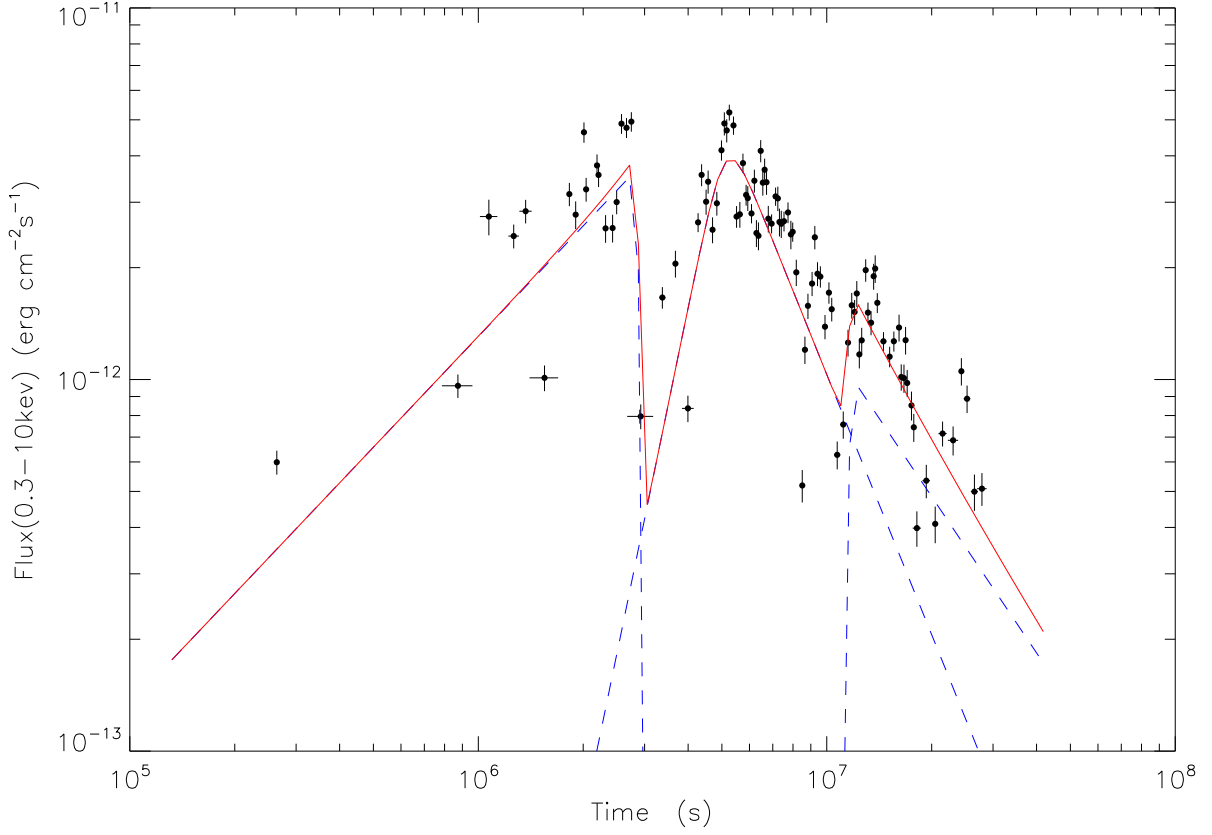


Fig. 2.— The best fit of three flares of Swift J1644+57 with three power-law functions after the subtraction of the underlying continuum. The start time is the start time minus 1.42×10^7 s. The red line shows the total best fit, and the dash lines show the best fits for individual flares.

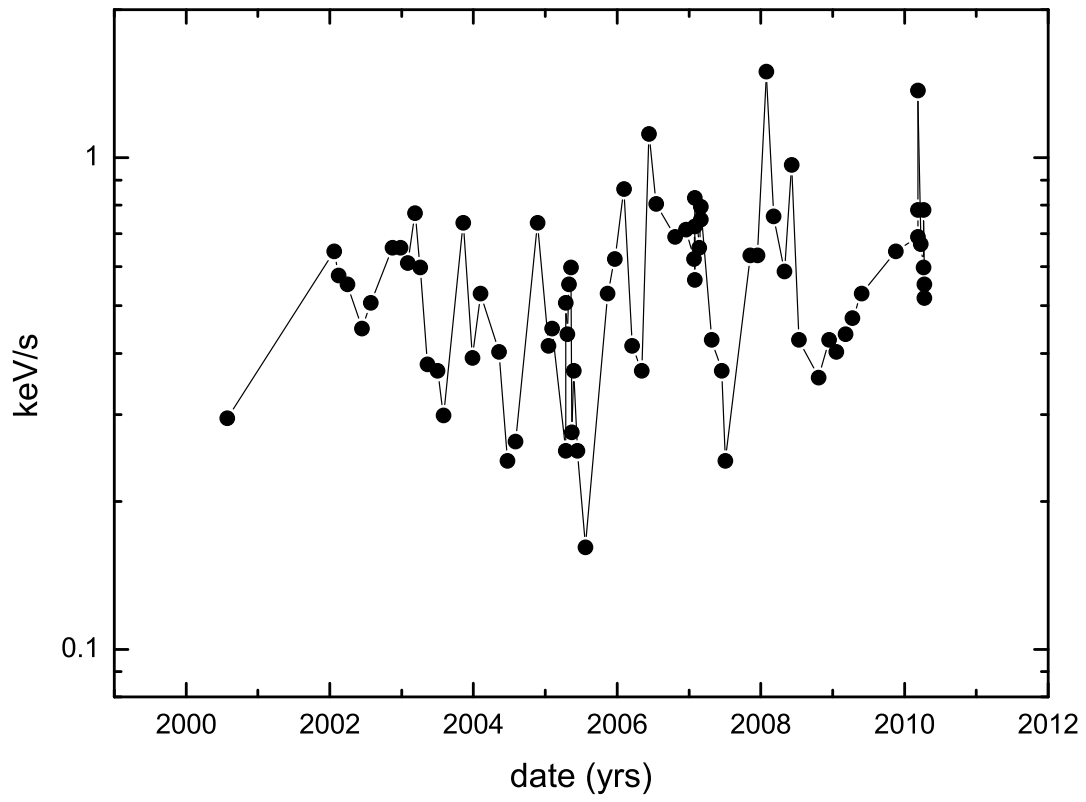


Fig. 3.— The X-ray light curve for the nucleus of M87 observed by Chandra.

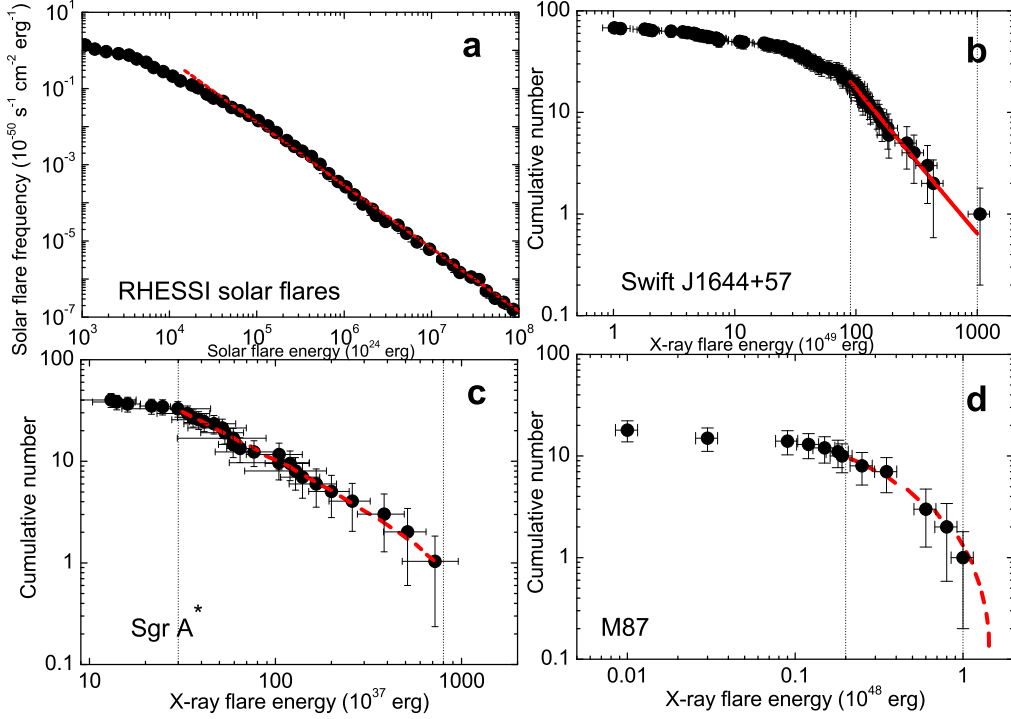


Fig. 4.— Cumulative size distributions of energy for X-ray flares. (a) The black dots are 11595 X-ray flares of the Sun observed by RHESSI. The red curve gives the differential energy distribution $dN/dE \propto E^{-\alpha_E}$, with $\alpha_E = 1.65 \pm 0.02$. (b) 68 X-ray flares from Swift J1644+57 are shown as black dots. The red curve gives the cumulative energy distribution $N(> E) = a + b[E^{1-\alpha_E} - E_{\text{max}}^{1-\alpha_E}]$ with $\alpha_E = 2.4 \pm 0.6$. The fitting range is between the two vertical dash lines. (c) 39 X-ray flares from Sgr A* observed by Chandra are shown as black dots. The red curve gives the best fit with $\alpha_E = 1.8 \pm 0.6$. The fitting range is between the two vertical dash lines. (d) 18 X-ray flares of M87 observed by Chandra are shown as black dots. The red curve gives $\alpha_E = 1.6 \pm 0.7$. The fitting range is between the two vertical dash lines.

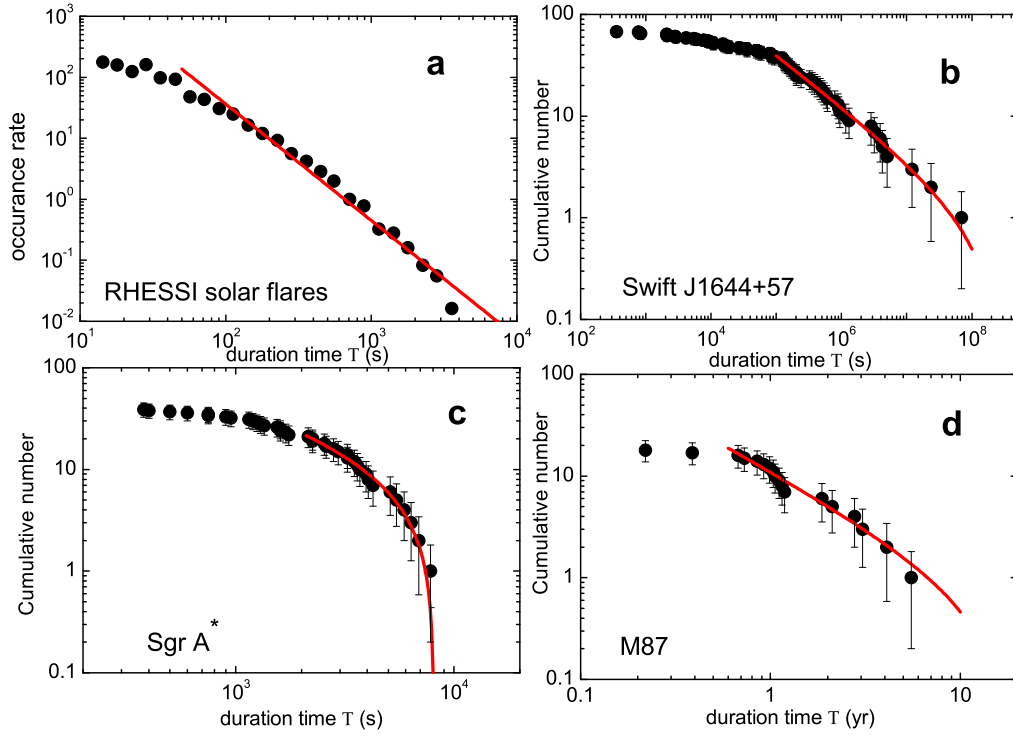


Fig. 5.— Cumulative size distributions of duration time. (a–d) The best-fit values of α_T are 2.00 ± 0.05 , 1.5 ± 0.6 , 1.9 ± 0.5 , and 2.0 ± 0.7 for solar flares, Swift J1644+57, Sgr A*, and M87, respectively. The fitting range is between the two vertical dash lines.

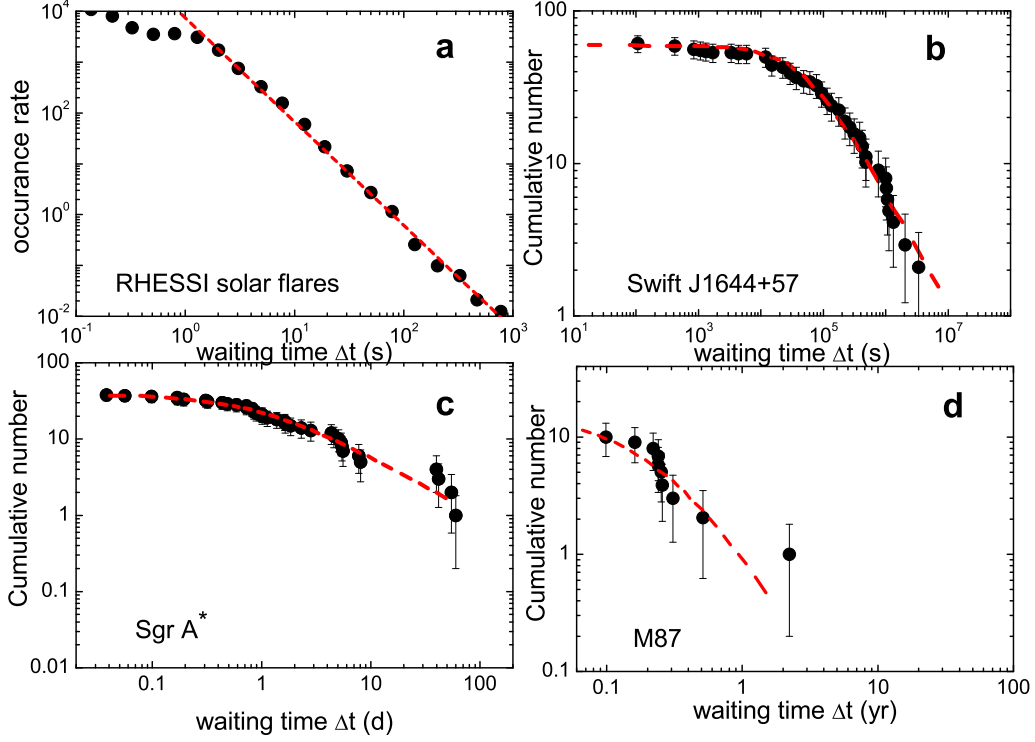


Fig. 6.— Cumulative size distributions of waiting time. (a–d) The best-fit power-law indices α_W are 2.04 ± 0.03 , 1.8 ± 0.6 , 1.8 ± 0.9 , and 2.9 ± 1.0 for solar flares, Swift J1644+57, Sgr A*, and M87, respectively.